

REVIEWS OF TOPICAL PROBLEMS

PACS number: **65.40. – b**

State-of-the-art and prospective materials for thermal barrier coatings

R.A. Shishkin

DOI: https://doi.org/10.3367/UFNe.2024.07.039716

Contents

1. Introduction **232**
2. Conventional and prospective materials **233**
3. Methods for applying thermal barrier coatings **234**
3.1 Comparison of spraying methods
4. High-entropy oxides **237**
4.1 Predicting stability of high-entropy compounds; 4.2 Properties of high-entropy ceramics; 4.3 High-entropy oxides
5. Conclusions **242**
Abbreviations **243**
References **244**

Abstract. **Gas-turbine engines are widely used in the electric power and aircraft industries. To reduce the extreme high-temperature load on combustion chamber elements, thermal barrier coatings are used: refractory ceramics sputtered on heat-resistant nickel alloys, which enables a significant reduction in the substrate temperature. An urgent task is to further increase the operating temperature of gas-turbine engines to enhance their efficiency. Due to the combination of physicochemical properties such as low thermal conductivity, the moderate thermal-expansion coefficient, and high thermal resistance and hardness, zirconium dioxide stabilized with yttrium oxide is conventionally used in industry. However, due to a phase transition in yttrium-stabilized zirconium dioxide (YSZ) occurring at operating temperatures, the working temperatures of gas-turbine engines cannot be further increased. To solve this problem, two major approaches are applied: further modification of zirconium dioxide (its doping) and the search for new alternative materials. By now, a vast set of candidates has been explored, including various complex oxides such as perovskites ($SrCeO_3$), pyrochlores ($La_2Zr_2O_7$), and fluorites ($La_2Ce_2O_7$). None of the examined materials in their original form can substitute for YSZ in gas-turbine engines. To optimize properties of new refractory materials, doping is used, the boundary case of which is the creation of high-entropy materials. By mixing five or more cations in the equiatomic proportion, extremely low thermal conductivity and enhanced thermal stability can be attained, so such materials are considered the most promising candidates for obtaining thermal-barrier coatings for next-generation gas-turbine engines. Basic materials and high-entropy oxides based on them, considered alternatives to YSZ, are reviewed.**

Keywords: thermal barrier coatings, zirconium dioxide, thermal conductivity, high-entropy oxides

R.A. Shishkin
Institute of Solid State Chemistry,
Ural Branch of the Russian Academy of Sciences,
ul. Pervomaiskaya 91, 620077 Ekaterinburg, Russian Federation
E-mail: shishkin@ihim.uran.ru

Received 27 December 2023, revised 5 July 2024
Uspekhi Fizicheskikh Nauk **195** (3) 245 – 259 (2025)
Translated by M.Zh. Shmatikov

1. Introduction

Significant dependence on imports of high-tech equipment and components has traditionally been a weakness of Russian industry and has become especially critical in the past decade. In particular, in the production of gas turbines, according to the Russian Ministry of Industry and Trade, the share of imports in 2014 was from 80 to 100%, and to date, no noticeable progress has been achieved in import substitution [1, 2]. The search for and creation of new materials that could be used in the production of gas turbine components seems to be an urgent research and practical task. Its solution will reduce the technological gap with Western countries in this area.

It is known that the efficiency of gas turbines is largely determined by their operating temperature: the higher the temperature, the higher the efficiency. Heat-resistant nickel alloys can operate at temperatures not exceeding 1000–1100 °C [3, 4]; therefore, to increase the operating temperature, refractory ceramic coatings with low thermal conductivity are used. Since the operating temperatures of gas turbine engines and new generation gas turbines exceed 1500 °C, stringent requirements have been set for the materials of all parts of gas turbines (structural, cooling systems, and thermal barrier coatings (TBCs)), which must be significantly improved [5] to achieve high efficiency.

Thermal barrier coatings (or thermal protection coatings) (Fig. 1) are innovative systems consisting of a metallic bonding coating and a refractory ceramic heat-insulating coating. The bonding sublayer protects against oxidative and corrosive effects, enhances the adhesion of the ceramic

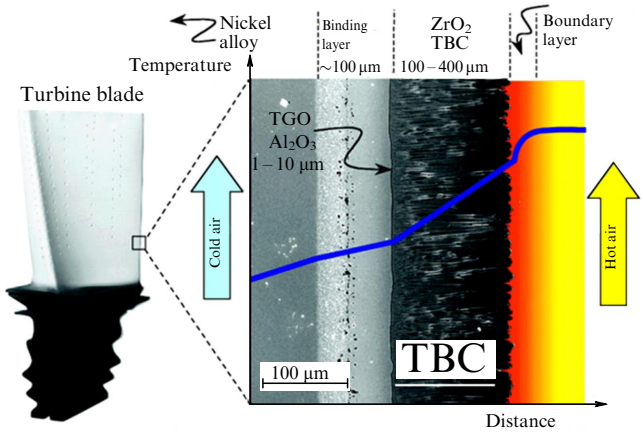

Figure 1. Schematic representation of thermal barrier coating [6].

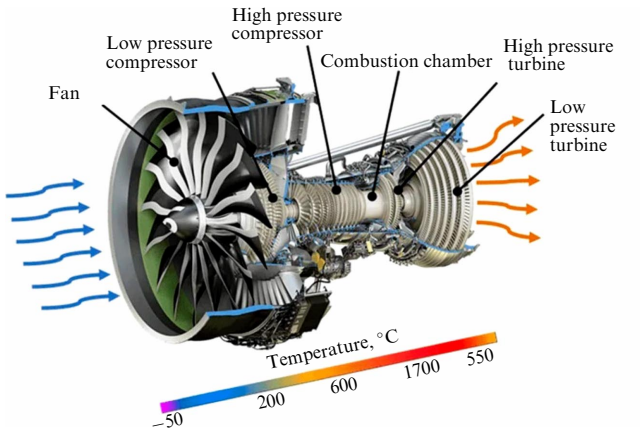

Figure 2. Diagram of gas turbine engine.

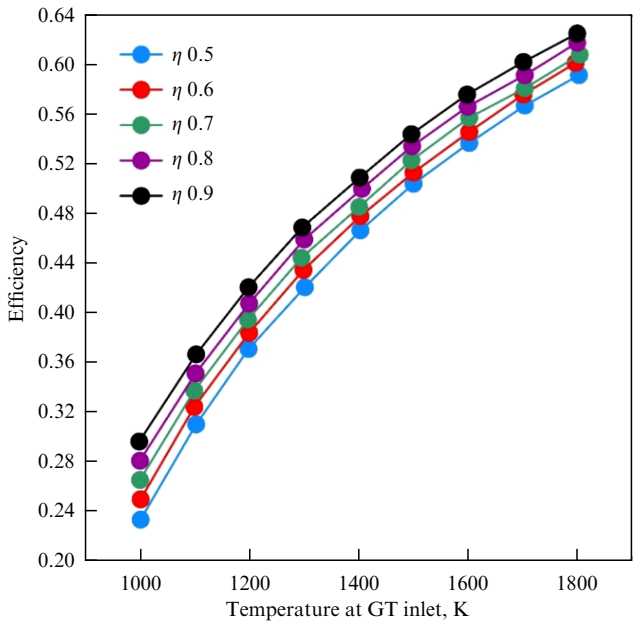

Figure 3. Dependence of gas turbine (GT) efficiency on gas phase temperature at gas turbine inlet at various intermediate cooler efficiencies η [9].

spray to the substrate, and compensates for the difference between the coefficients of thermal expansion of the substrate and ceramic materials. However, refractory materials feature a significantly lower thermal conductivity than that of the substrate, which, in the presence of external cooling systems (for example, blowing cold air along the outer contour of the hot part of the engine), leads to the emergence of a high temperature gradient (a difference of 50–300 °C) in the ceramic thermal insulation coating.

TBCs are usually applied in the hot section of gas turbine engines to coat such parts as combustion chamber walls, turbine blades, nozzles, etc. (Fig. 2).

There are two approaches to enhancing the economic efficiency of engines. The first is to reduce the operating temperature of structural metal parts, thereby extending their service life and, as a result, increasing the average number of hours before major repairs to the turbine. The second approach is to increase the combustion temperature of the fuel in the hot section of the gas turbine, which will lead to an increase in efficiency (Fig. 3) [8].

2. Conventional and prospective materials

Based on the above, stringent requirements were formulated for TBCs, which are presented in Table 1 [10, 11].

The most common material used in the industry as a TBC is zirconium dioxide, partially stabilized with 6–8 mol % yttria (YSZ), which features high hardness (6.5 GPa according to Vickers) [12], an acceptable coefficient of thermal expansion ($10-11.3 \times 10^{-6}$ K^{-1}), and low thermal conductivity (about 2.0–2.7 W m^{-1} K^{-1}) at elevated temperatures [10, 11, 13]. However, during long-term operation of gas turbines with a YSZ coating, a phase transformation of the metastable tetragonal (t′) phase into the tetragonal (t) and cubic (c) phases occurs [10, 11]. Upon cooling, the tetragonal (t) phase transforms into the monoclinic phase, which is accompanied by an increase in volume by approximately 4%, resulting in internal stresses that lead to cracking of the coating. Another adverse feature of YSZ coatings is the sintering of zirconium dioxide particles at temperatures above 1200 °C, leading to a decrease in porosity. This enhances the thermal conductivity of the TBC, which leads to an increase in the substrate temperature. The use of solid solutions based on zirconium dioxide [14] makes it possible to increase the hardness of the material to 12.0 GPa and the thermal expansion coefficient (TEC) to 12.2×10^{-6} K^{-1} when doped with titanium dioxide; however, this approach does not prevent the phase transition.

One of the common approaches to improving the phase stability and reducing the thermal conductivity of zirconium oxide is the use of simultaneous co-doping with several cations (Fig. 4), such as yttrium, ytterbium, gadolinium, tantalum, scandium, lanthanum, and other rare and rare earth metals [15–19]. It has been shown that the introduction of lanthanum, cerium, and yttrium oxides, in addition to the phase stabilization of zirconium dioxide, simultaneously increases the corrosion resistance of TBC in calcium-aluminosilicate melts. This effect is explained by the fact that, when rare earth metal cations dissolve in the CMAS melt, a phase with an apatite crystalline structure is formed, which prevents further penetration of silicates [20].

In essence, the method of introducing a large number of dopants is a way of entropic stabilization of zirconium dioxide. A new direction in materials science based on the creation of new materials due to high configurational entropy is considered below. However, if the dopant content is small, the increase in configurational entropy is insignificant also

Table 1. Required properties of TBC materials.

Parameter	Meaning
Melting point, °C	> 2000
Thermal conductivity, W m^{-1} K^{-1} Dense ceramics Coating	 < 2.5 0.9–1.2
Temperature range of phase stability, °C	25–1500
Thermal expansion coefficient (TEC), 10^{-6} K^{-1}	10–15
Oxygen conductivity	Low
Corrosion resistance to calcium–magnesium–alumino-silicates (CMAS)	High
Adhesion to substrate material	High
Crack resistance (coefficient K_{1c}), MPa m$^{1/2}$	> 1.0

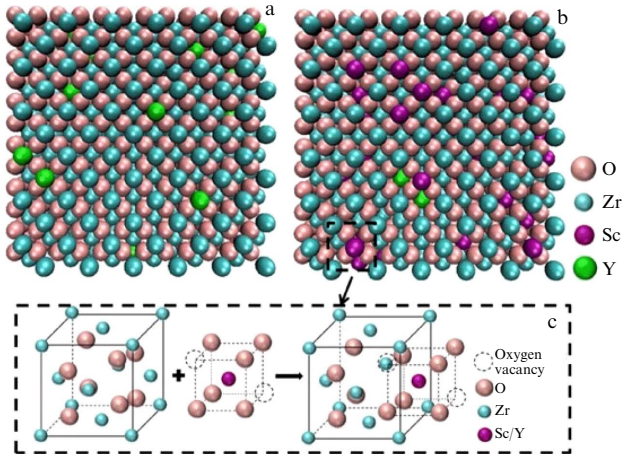

Figure 4. Distribution of ions in (a) YSZ and (b) scandium-doped YSZ; (c) schematic of replacement of Zr^{4+} ions with Sc^{3+} and Y^{3+} [16].

compared to the equiatomic ratio of components, which is the main trend in the creation of new high-entropy ceramics (HECs).

Another approach to the creation of TBCs is to search for new, alternative materials, to which a large number of studies have been devoted in recent years [11, 21–24]. Modern studies consider as an alternative oxides of rare (HfO_2-18% Y_2O_3) [25] and rare earth metals La–Ce–Ta–O [26]), zirconates, hafnates, tantalates with a pyrochlore structure ($RE_2M_2O_7$, RE = La – Gd, M = Hf, Zr, Fe–Ta) [11, 13, 27–33], cerates with a fluorite structure ($RE_2Ce_2O_7$) [33–35], monosilicates RE_2SiO_5 (RE = Gd, Y, Er) [36], molybdates $La_2Mo_2O_9$ [37, 38], perovskites ($SrZrO_3$, $BaZrO_3$, $SrCeO_3$) [10, 39–41], and other complex oxides $Ca_3Ln_3Ce_7Ta_2O_{26.5}$ (where Ln = Gd, Yb) [42].

Despite high hardness (12.21 GPa) and low thermal conductivity (0.9 W m^{-1} K^{-1} for the applied coating with a porosity of 12.9%), yttria-stabilized hafnium dioxide possesses too low a TEC value (9.24×10^{-6} K^{-1}) [25]. Highly porous coatings (13.18–20.58%) made of the complex oxide La–Ce–Ta have low thermal conductivity (0.35–0.5 W m^{-1} K^{-1} in the temperature range up to 1200 °C) and sufficient hardness (2.5–4.25 GPa); however, the TEC does not exceed 10×10^{-6} K^{-1} in the temperature range up to 1600 °C [26]. Compounds with a pyrochlore structure have a low thermal conductivity of 2.15 W m^{-1} K^{-1} at 1000 °C, sufficiently high melting point (1977–2027 °C), sufficient hardness of 9.9 GPa, but low TEC value ($7.6-10 \times 10^{-6}$ K^{-1} in the range from 100 to 1100 °C). The best combination of properties among compounds with a pyrochlore structure is exhibited by $Gd_2Hf_2O_7$ [13] with a TEC of 12×10^{-6} K^{-1} and thermal conductivity of 1.5–1.8 W m^{-1} K^{-1}. However, due to expensive reagents, the economic feasibility of using such coatings is extremely low. Due to the combination of extremely low thermal conductivity (0.8–1.0 W m^{-1} K^{-1}) and high TEC values (15.36×10^{-6} K^{-1} at 500–600 °C), $La_2Mo_2O_9$ is an extremely interesting material for TBC, but the presence of a phase transition α-$La_2Mo_2O_9$ to β-$La_2Mo_2O_9$ occurring at 577 °C, accompanied by a rapid increase in TEC to 31.0×10^{-6} K^{-1} [37, 38], ruled out its practical application.

Compounds with a perovskite structure (ABO_3) are of the greatest interest due to their attractive physicochemical properties. Barium and strontium zirconates feature a high melting point and low thermal conductivity [43–45], but $BaZrO_3$ has an immense drawback: a low TEC ($6.2-7.8 \times 10^{-6}$ K^{-1}) [45, 46], while $SrZrO_3$ has several polymorphic modifications and undergoes a number of phase transformations in the temperature range of 750–1130 °C [44, 47, 48]. Study [10] has shown that strontium cerate is a highly promising material, featuring a higher TEC than strontium zirconate (11.1×10^{-6} K^{-1}) [10, 49], no phase transformations up to and including 1500 °C, and a thermal conductivity of less than 3.0 W m^{-1} K^{-1} [10, 44, 45] at temperatures up to 1000 °C. In [50], it was shown that replacing 5 mol % cerium with tin or yttrium, on the one hand, allows increasing the TEC value to 11.3×10^{-6} K^{-1} and the hardness of sintered ceramics (relative density 85–87%) from 1.5 to 4.5 GPa, but, on the other hand, reduces the thermal conductivity of dense ceramics to 1.8–2.0 W m^{-1} K^{-1} at 1000 °C.

A conceptual comparison of alternative materials for TBCs is displayed in Table 2. Based on the presented data, it may be concluded that the most promising materials are those with a perovskite-like structure.

3. Methods for applying thermal barrier coatings

Elements of the hot section of gas turbine engines are made of heat-resistant alloys Haynes 230, Hasteloy X, or their Russian analogues ZhS-32 VI and ZhS-6U [21, 22]. To enhance the adhesion of sprayed coatings, they are usually subject to sandblasting, which allows increasing the service life of TBCs to 600–750 cycles. NiCrAlY or NiCoCrAlY alloys are usually used as a sublayer for TBC, although it is worth mentioning that using high-entropy alloys as a sublayer for TBC has gained particular popularity [69–71]. The thickness of the bonding layer ranges from 75 to 150 μm.

Two main methods for producing TBCs are applied (Fig. 5): atmospheric plasma spraying (APS) and physical vapor deposition by electron beam evaporation (EB-PVD) [72]. In recent years, the method of applying TBC using high-velocity oxy-fuel spraying (Fig. 5c, HVOF) has been actively developed [73–75].

3.1 Comparison of spraying methods

3.1.1 Initial materials. One of the main problems of the APS and HVOF methods is the need to use a spherical (flowing) powder with a given narrow particle size distribution (usually 40–60 μm for APS), for which particle spheroidization methods can be used, such as spray drying or particle melting in plasma [77–80]. One of the promising approaches that

Table 2. Comparison of materials for TPCs.

	λ at 1000 °C, W m^{-1} K^{-1}	TEC at 1000 °C, 10^{-6} K^{-1}	Phase stability	Hardness, GPa
YSZ [10, 11]	1.6–2.5	10.4–11.0	–	13–15
YSH [51, 52]	2.0–3.0	9.2	–	8–9.3
$La_2Zr_2O_7$ [11, 53]	2.0	8–10	+	8.3
$RE_2Zr_2O_7$ [11, 28, 54, 55]	0.76–1.5	11.5	+	8.8–10.0
$RE_2Ti_2O_7$ [56, 57]	1.75–2.25	10–11	+	15–16
$RE_2Ce_2O_7$ [33, 58]	1.2–1.7	11.7–12.2	+	3.5
$Gd_2Hf_2O_7$ [59, 60]	1.4–1.8	12.0		17.1
$Ca_3RE_3Ce_7Ta_2O_{26.5}$	1.8	11.4–11.7	+	Unknown
$BaZrO_3$ [46, 61]	3.5	7.1	+	7.2–11.1
$SrCe_{1-x}Sn_xO_3$ [62]	1.2–1.6	11.6–12.4	+	4.5
$La_2Mo_2O_9$ [37, 38, 63]	0.8–1.0	15.36	–	Unknown
RE_2SiO_5 [64, 65]	1.5	8.4	+	5.3
$RE_2Si_2O_7$ [66, 67]	2.0	3.9	+	6.2
$LaMgAl_{11}O_{19}$ [68]	2.4	8.5	+	14.4

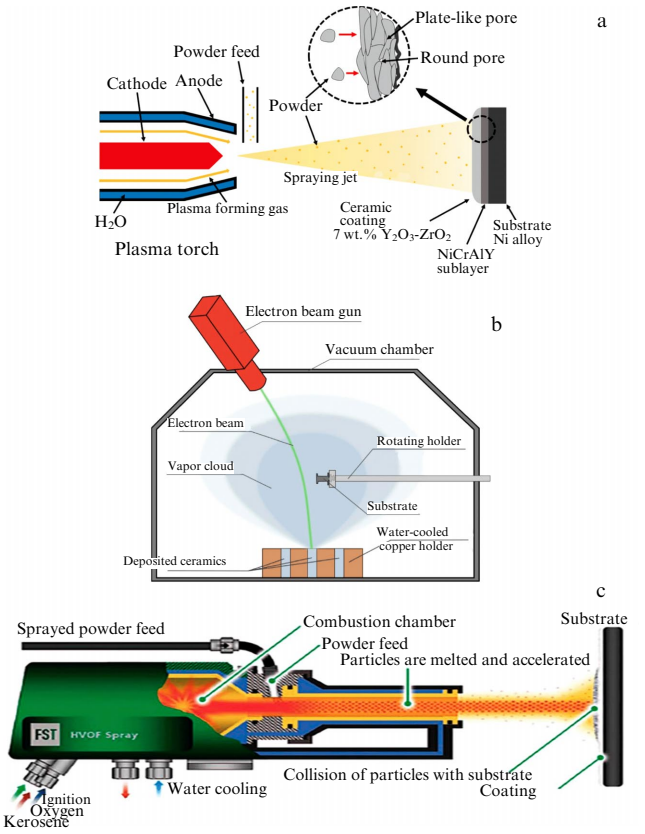

Figure 5. Main methods of applying thermal barrier coatings: (a) atmospheric plasma spraying [76]; (b) electron beam spraying; (c) high-velocity flame spraying [74].

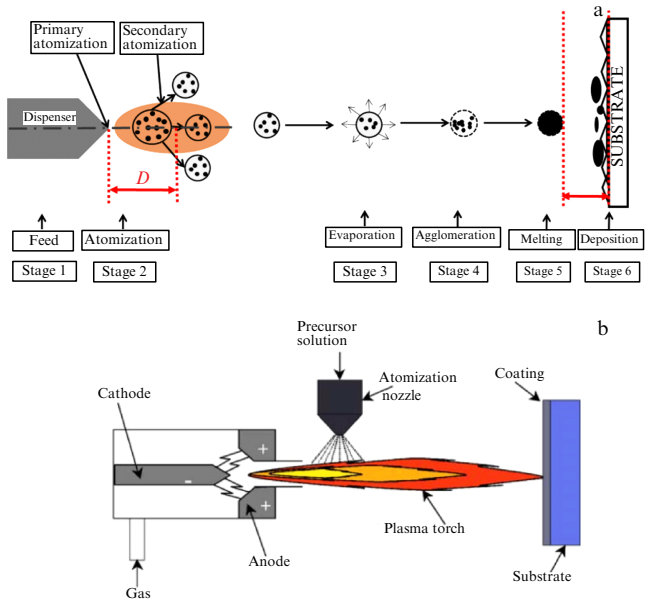

Figure 6. Schematic images of processes (a) SPS [83, 84] and (b) SPPS [85].

allows the use of small particles, less than 10 μm, including nanodispersed powders with complex particle morphology, is suspension spraying (in plasma — suspension plasma spraying, SPS (Fig. 6), or in a combustion chamber — suspension high velocity oxy fuel, S-HVOF) [75, 81, 82]. As a development of the SPS method, it was proposed to use a precursor for spraying, which forms the required material in the *in situ* application process. This method is called solution precursor plasma spraying (SPPS) (Fig. 6b). However, since unreacted precursor often remains when using SPPS, SPS and S-HVOF are more attractive as promising TBC spraying methods.

The EB-PVD method uses ceramic blanks, which significantly simplifies the stage of preparing ceramic materials for spraying.

3.1.2 Microstructure and surface roughness. During plasma spraying, the powders of the initial raw materials melt and are rapidly applied to the substrate to form a flattened particle. The process occurs through the successive collision and

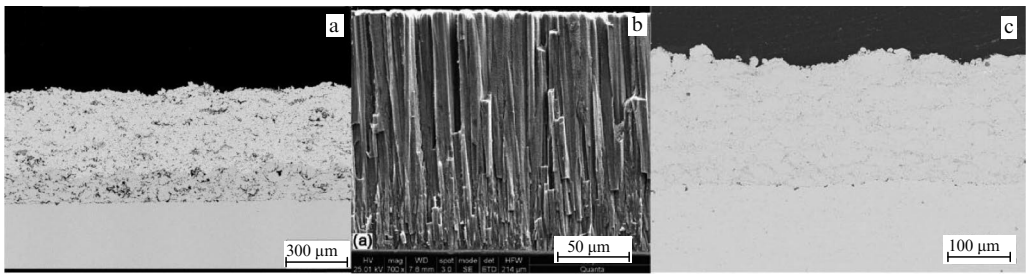

Figure 7. Image of microstructure of coatings applied by (a) APS [94], (b) EB-PVD [95], and (c) HVOF [89].

interweaving of these particles, which results in a lamellar structure (Fig. 7a) [86]. The electron-beam deposition leads to the formation of a columnar microstructure, which is considered more resistant to deformation, erosion, and temperature changes (Fig. 7b). It is worth noting that, when using powder suspensions (SPS), the microstructure of the resulting coatings is similar to the structure of EB-PVD TBC, which allows setting alternating layers with their own unique morphology directly during the plasma spraying process in one technological process [81].

Due to the high pressure created by the mixture of flammable gas and oxygen in the combustion chamber, the powder particles acquire a high velocity with which they collide with the surface of the substrate. The coating obtained by the HVOF method, similar to APS, is a layered structure consisting of highly deformed particles. However, the HVOF method yields denser coatings with a lower content of melted particles than APS (Fig. 7c).

Another important parameter is the surface roughness of the applied coatings: it is generally accepted that, the lower the roughness, the smaller the hydrodynamic resistance of the blades of a gas turbine engine [87]. However, modeling the operating conditions of gas turbine engines shows that their overall efficiency does not depend on the surface roughness. The effect of surface roughness on turbine performance depends on the wall curvature: for flat walls, the highest efficiency is achieved with a smooth surface, while a rough surface provides the best results on convex walls at low blowing coefficients or on concave walls at high blowing coefficients [88].

The EB-PVD method yields a less rough surface (~ 1 μm) than APS (~ 10 μm) [81]. TBCs obtained using HVOF also allow achieving low surface roughness (5–10 μm) [89]. To reduce the surface roughness of the coatings, mechanical polishing or melting due to high-temperature treatment with a plasma torch or laser can be used [90]. TBCs with low surface roughness retain an aerodynamically advantageous smooth surface and usually feature a longer service life [91].

The strength of adhesion between the substrate and TBC for the EB-PVD method is 10 times higher (~ 400 MPa) than for TBC obtained by plasma spraying (20–55 MPa, for YSZ), which is an important factor in preventing premature spalling of the YSZ layer [92]. One of the main advantages of the HVOF method over APS is the high adhesion strength (70 MPa) combined with minimal thermal impact on the substrate [93].

3.1.3 Porosity of coatings. The thermal properties of TBCs, in addition to the material being sprayed, depend to a large extent on porosity, which in turn is inextricably linked with the previously discussed microstructure of the coating. Porous TBCs can dramatically reduce the temperature of metal substrates by 100–300 °C, depending on the thickness of the thermal insulation ceramic coating (the thicker the thermal insulation layer, the lower the temperature that can be achieved directly on the blade of a gas turbine engine) and the microstructure (columnar crystals or isotropic porous coating).

Study [96] showed that the porosity enhanced due to an increase in the degree of particle fragmentation leads to a decrease in thermal conductivity, which ensures high resistance to deformation for TBCs. However, although high porosity provides better thermal protection, the service life of the coatings is limited by oxidation of the metallic binder layer (formation of thermally grown oxide) due to oxygen penetration through crack channels and by direct oxygen transport through the coating, which causes its delamination. Oxygen diffusion from the gas phase to the binder layer is especially important for columnar particles obtained by the EB-PVD method; to solve the problem of oxygen diffusion, as in the case of reducing roughness, the TBC surface can be partially melted.

The open porosity of TBC is extremely harmful due to the infiltration of corrosive substances and CMAS into the pores during the operation of gas turbine engines [11, 20, 58], which leads to a reduction in their service life before major repairs.

On the other hand, the mechanical properties of materials significantly depend on their porosity [97], which implies that such coatings are more resistant to the abrasive effects of foreign particles that can get into the engine. At the same time, small closed pores with sizes ranging from 0.02 to 1 μm can prevent crack propagation.

The porosity of coatings obtained by the EB-PVD method (up to 18%) is comparable [98] to that of APS coatings (2–20% [93, 99]). However, the porosity of coatings applied by the HVOF method is an order of magnitude less than that for APS (up to 0.2%) [93], which, as mentioned earlier, yields greater hardness and, at the same time, larger thermal conductivity of the coatings.

When using suspensions, the porosity of the coatings can increase slightly; for example, the S-HVOF method allows obtaining coatings with lower porosity, 1–3%; SPS, 4–15% [82], and SPPS, 15–25%. Despite approximately the same productivity and powder utilization efficiency (around 50%), due to the larger amount of expensive gases consumed in the S-HVOF (H_2–O_2) process, the cost of applying coatings by the high-velocity flame spraying method is approximately twice as high as for atmospheric plasma spraying [82].

Thus, ideal coatings feature a small porosity (10–20% [99]) without through pores, with minimal oxygen transport and resistance to oxidation, corrosion, and thermal shock.

Table 3. Properties of TBCs deposited using different techniques [93, 100–106].

Property	EB-PVD	APS	HVOF
Thermal conductivity, W m^{-1} K^{-1}	1.5–1.9	0.8–1.1 (1.8*)	0.8–2.0
Porosity, %	< 18	2–20	0.2–20
Surface roughness, μm	1	10	5–10
Adhesion to substrate, MPa	400	20–40	70
Microhardness, MPa	5.5	5.2	5.5
Modulus of elasticity, GPa	90–150	200	80–130
Coating thickness, μm	< 350	< 400	< 1000
Coating growth rate, kg h^{-1}	< 10–15	< 10	< 9
* Thermal conductivity increases due to sintering of YSZ coating.			

Table 4. Methods of TBC deposition [81].

Method	Shape of the deposited material/ Resulting microstructure	Characteristics	Equipment	Challenges
EB-PVD	Sintered columns/Homogeneous columnar microstructure	Low deposition rate (1–2 μm min^{-1}). Virtually no impurities are introduced. Good heat transfer. Low roughness.	Extremely expensive	Filament destruction leads to uneven evaporation. Not all materials are suitable for EB-PVD evaporation.
APS	Flowable (spherical) powders with particle size of 5–100 μm/ Porous microstructure with large number of defects, suitable for high-temperature applications.	A variety of substrates can be used (metal, ceramics, glass, composites)	Cheaper than EB-PVD	Influence of a large number of parameters on spraying process. Problems with spraying on forms and surfaces with complex geometry. Frequent replacement of plasma torch electrodes to maintain uniform quality of coatings.
SPS	Submicron or nanoparticle suspension/Columnar, similar to EB-PVD	Higher values of permissible deformation, which allows a greater number of thermal cycles.	Special feeder is required to work with liquid	Complex technological process due to use of liquid (suspension). Influence of a large number of parameters on spraying process, which are currently poorly understood. Feed of sprayed material and, accordingly, spraying rates are 2–3 times lower than with APS. Shorter distance to the target leads to an increase in heat flux density (20 MW m^{-2}).

A comparison of the main application methods is presented in Tables 3 and 4. The most promising technique for applying TBC can be considered SPS, which enables a significant simplification of the coating application technology: submicron and nanosized powders of complex morphology can be used while maintaining a high spraying rate. Moreover, the same SPS equipment can be used for plasma melting of the surface of the deposited coatings (similar to laser melting described in [90]), thereby eliminating the through porosity characteristic of columnar crystals and reducing the roughness of the TBC.

4. High-entropy oxides

In 2004, solid solutions with a large number of components were proposed as a new class of materials. The idea was to maximize the configurational entropy to stabilize equimolar mixtures and obtain more stable compounds, which became known as high-entropy materials. High-entropy ceramic materials are a solid solution with a single crystal lattice, which includes more than five elements. The enhanced stability of HECs is primarily due to the change in the Gibbs free energy during the formation of a solid solution (G_{mix}) [107]:

$$\Delta G_{mix} = \Delta H_{mix} - T\Delta S_{mix}, \quad (1)$$

where H_{mix}, S_{mix} are the enthalpy and entropy of mixing and T is the absolute temperature. As entropy increases, the Gibbs energy decreases, i.e., the compound stabilizes.

Entropy is a thermodynamic parameter that reflects the degree of disorder in a material. Entropy is affected by various factors, such as magnetic moment, atomic vibration, and the arrangement of atoms in the crystal lattice. It is the last factor that has proven to be the most effective to stabilize compounds. Entropy is also affected by temperature, the number of elements, and the atomic fraction of each element in the composition. The relationship between the atomic

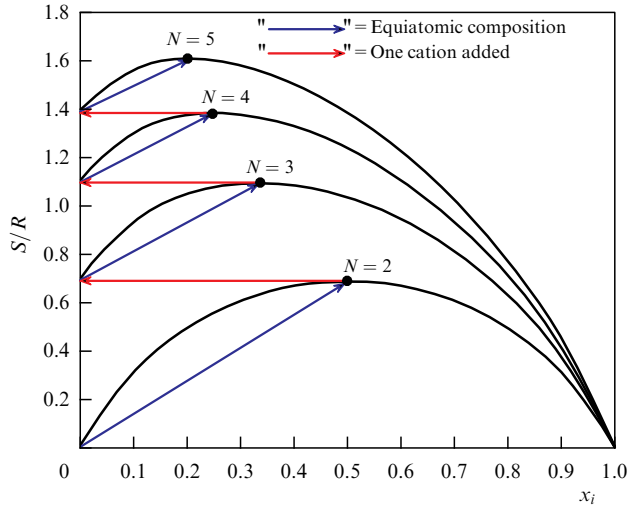

Figure 8. Change in configurational entropy depending on composition of solid solution with n cations [108].

fraction of elements and the entropy of mixing is shown by the following equation [107, 108]:

$$\Delta S_{\text{mix}} = -R\sum_{i=1}^{N} x_i \ln x_i\,, \tag{2}$$

where R is the gas constant, x_i is the atomic fraction of the ith element, and N is the total number of elements.

The entropy of mixing reaches its maximum with an increase in the number of elements: when they are in an equiatomic ratio, the entropy of mixing takes the form

$$\Delta S_{\text{mix}} = R\ln N\,. \tag{3}$$

Several different definitions for high-entropy materials can be found in publications [107]:

- the presence of at least five elements, the concentration of each is in the range of 5–35 at. %;
- the entropy of mixing is greater than $1.5R$;
- the entropy of mixing is greater than $1.61R$ (Fig. 8).

The last is based on the observation that at values $\geqslant 1.61R$ the contribution of the entropy factor ($T\Delta S_{\text{mix}}$) can exceed that of enthalpy (H_{mix}), yielding a negative Gibbs free energy of obtaining a single-phase compound. However, several clarifications regarding the HEC terminology [107] would be relevant:

- the compound must be single-phase (although sometimes researchers include two-phase compounds in this group);
- despite the term 'high-entropy,' such ceramics often have an ordered structure, but nevertheless with a high entropy value, which is relatively common for ordered ceramics;
- many studies devoted to multicomponent systems use the term HEC in relation to the large number of various elements;
- entropy stabilization is observed not only in high-entropy ceramics ($\Delta S_{\text{mix}} \geqslant 1.5R$) but also for medium-entropy ceramics (3 or 4 cations with $R \leqslant \Delta S_{\text{mix}} < 1.5R$) and in some multicomponent systems.

In choosing the cations to be included in the composition of HECs, it is believed that there are two main factors that must be taken into account:

- geometric compatibility: the sizes of the cations should not differ greatly (data are reported on a maximum difference of 5, 10, and even 18%, at which single-phase compounds are still formed);
- electric neutrality: the charge of the metal cations should be equal to that of the anions.

Initial studies focused primarily on metal alloys and nitride films. In 2015, entropic stabilization was demonstrated in a mixture of oxides. Then, the rapid development of high-entropy ceramics technology stimulated the addition of more components to obtain materials with a combination of different properties. Currently, a large number of various high-entropy compounds are known (Fig. 9).

4.1 Predicting stability of high-entropy compounds

To predict the structure of a high-entropy material, empirical models using *descriptors* are considered along with the calculation of the Gibbs free energy. A descriptor is a parameter whose value is used to predict the possibility of forming a high-entropy compound (e.g., the tolerance factor for perovskites).

Calculating the Gibbs free energy provides quantitative information about the phase stability. The Gibbs free energy is calculated in several ways: using the density functional theory (DFT), molecular dynamics simulation, or phase diagrams. DFT-based methods are considered optimal for calculating the energy given the chemical complexity of high-entropy materials. The addition of each element to high-entropy ceramics can significantly affect their crystal structure. DFT calculations are efficiently used to clarify the contribution of individual elements to the crystal structure of high-entropy oxides.

However, the problem with DFT-based methods is that they are computationally expensive due to the large number of equations, which significantly increases the calculation time.

In addition, high-entropy materials with randomly distributed states and several elements cannot be accurately analyzed using DFT. Unlike density functional theory, the calculation time of molecular dynamics simulations is shorter, so this method is suitable for materials with more than five metals in the B-sublattice. The main disadvantage of molecular dynamics simulations is that they disregard interatomic potentials in the calculation. Recently, due to technical advances, a combined method has become the most common technique for calculating the Gibbs free energy. The combined method allows using DFT calculations of interatomic potentials, thereby complementing the simulation. To quickly assess the possibility of HEC formation, descriptors — tools that can describe the possibility of obtaining a single-phase high-entropy compound — are often used. Below, several types of descriptors are described that are actively employed to predict the stability of high-entropy compounds.

For perovskite-like materials, the tolerance factor can be used as a descriptor. Calculations showed that the tolerance factor for all single-phase perovskites is close to one ($0.97 \leqslant t \leqslant 1.03$). Consequently, a tolerance factor close to unity is necessary for the formation of a single-phase high-entropy perovskite [110].

For high-entropy oxides with a fluorite structure, it was proposed to use the standard deviation of the cation sizes (s) in one sublattice as a descriptor. If the standard deviations of the cationic radius distribution are greater than 0.095, fluorite

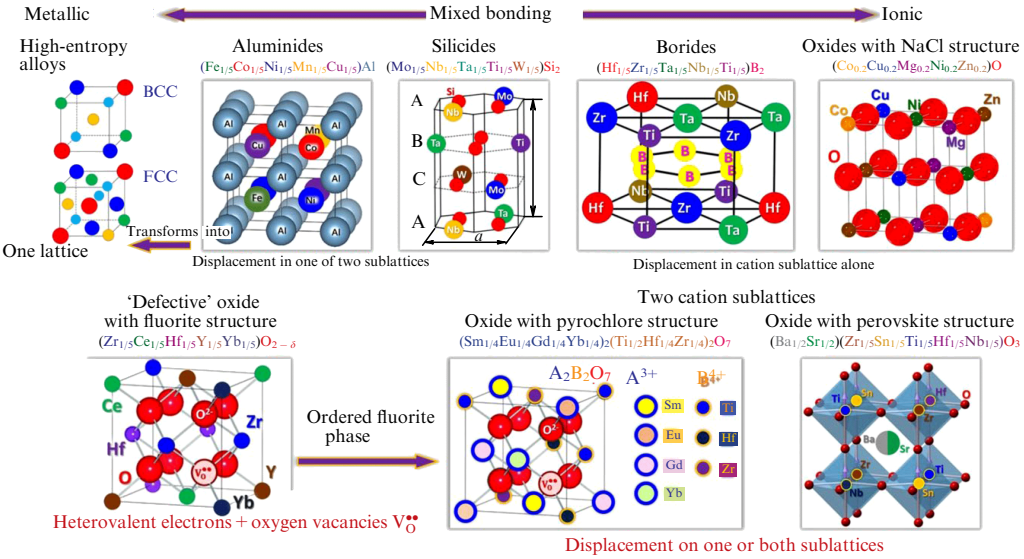

Figure 9. Schematic representation of known structures of high-entropy compounds [109].

is single-phase. When the standard deviation is less than 0.095, a mixture of fluorite and bixbyite or single-phase bixbyite is formed [111]:

$$s = \sqrt{\frac{\sum_{i=1}^{5}(r_i - \bar{r})^2}{5-1}}, \tag{4}$$

where $\bar{r}$ and r_i are the average radius and the radius of the ith component, respectively. A descriptor similar to the standard deviation is the $\delta(R)$ parameter. This descriptor is often used to describe the difference in cation sizes in one of the sublattices of complex compounds; next, a clarification is given as to which of the sublattices the calculation refers, for example, $\delta(R_A)$ or $\delta(R_B)$ [112, 113]:

$$\delta(R_B) = \sqrt{\sum_{i=1}^{5} c_i \left(1 - \frac{r_i}{\bar{r}}\right)^2}, \tag{5}$$

where c_i is the concentration of the ith component. Another descriptor for the pyrochlore structure is the size disorder factor:

$$\delta^*_{size} = \sqrt{\delta_A^2 + \delta_B^2}, \tag{6}$$

where δ_A and δ_B are the difference between cation sizes in sublattices A and B of the pyrochlore lattice, associated with sites A and B in the pyrochlore structure. It turns out that, to predict thermal conductivity, the disorder factor is more effective as a descriptor than is the entropy of ideal mixing. The results showed that thermal conductivity decreases with an increase in the size disorder factor due to the significant effect of lattice distortion on the decrease in thermal conductivity (Fig. 10).

4.2 Properties of high-entropy ceramics

Significant interest in HECs also arose after the publication of the properties of the entropy-stabilized oxide $(Co_{0.2}Cu_{0.2}Mg_{0.2}Ni_{0.2}Zn_{0.2})O$ [114]. Since then, the number of studies in which various classes of high-entropy compounds (carbides, nitrides, borides, sulfides, silicides) were obtained and their properties examined has rapidly increased [4, 107, 109, 115]. Low thermal conductivity, associated with distortions of the crystal lattice, is comparable to that of amorphous materials. Due to this and increased hardness, such materials are promising candidates for use as thermal barrier (heat-insulating) coatings. The improvement in mechanical properties is due to the effect of solid solution strengthening when introducing a large number of elements with different ionic radii, Hall–Petch strengthening (the nanograin structure slows down the movement of dislocations), and the modification or disappearance of slip planes. Inhibition of grain growth at high temperatures is attributed to distortions in the crystal lattice, which increase the energy of the crystallites. High-entropy carbides were used as an example to show that the elastic modulus and hardness depend on the valence electron density [116]. This observation can probably be approximated for other compounds, since an increase in hardness is also observed for other chemical classes of high-entropy compounds [117, 118]. It is often difficult to establish the cause of the change in the properties of HEC, making researchers resort to computer modeling methods [115].

The most detailed study of the thermophysical properties of high-entropy compounds was carried out for complex oxides with a pyrochlore structure. It showed that an increase in entropy in any of the sublattices (the A sublattice of a rare earth metal or the B sublattice of a transition metal) leads to a decrease in thermal conductivity. However, the greatest decrease is usually observed with an increase in entropy in both lattices concurrently (Fig. 10a). The greatest decrease in thermal conductivity and an increase in the elastic modulus of high-entropy ceramics occur with an increase in the difference between the sizes of cations that form a solid solution (Fig. 10b, c); an almost linear increase is observed with maximum values attained near the stability boundary of the high-entropy structure.

It is of interest that the presence of oxygen vacancies (Fig. 11) insignificantly affects the properties of the resulting compounds, while an increase in thermal conductivity is observed due to the growth of the electronic component responsible for electrical conductivity.

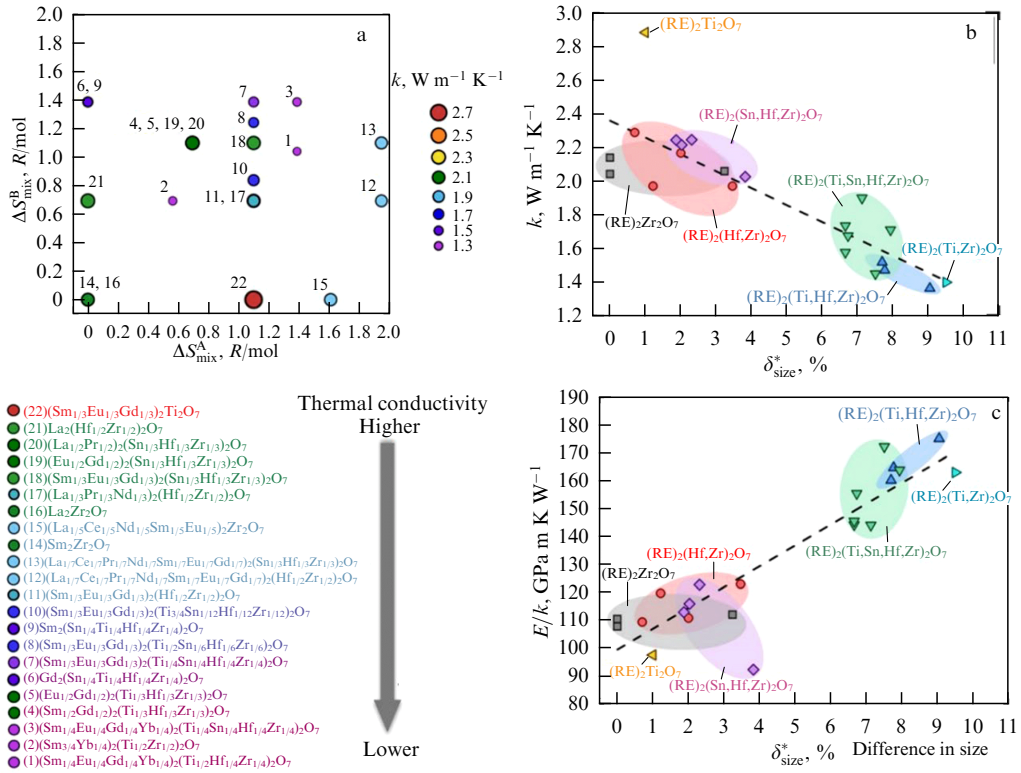

Figure 10. (a) Measured thermal conductivity of 22 high-entropy pyrochlores and (b) relation between thermal conductivity and (c) ratio of elastic modulus to thermal conductivity and size difference of cations in sublattices [109].

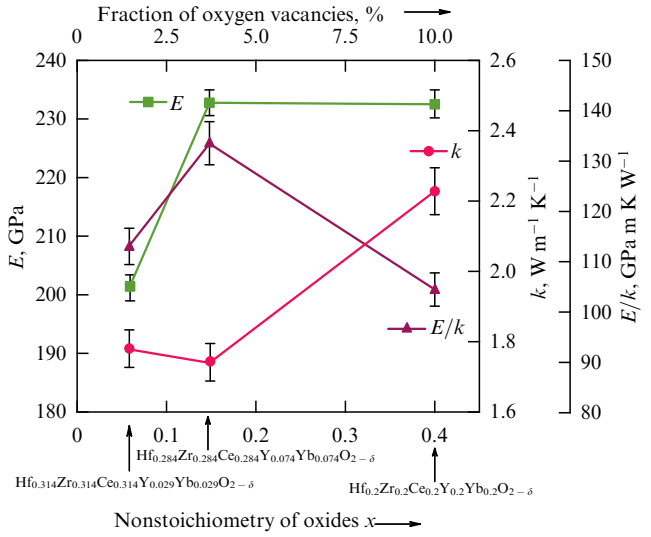

Figure 11. Relationship between measured thermal conductivity and elastic modulus and nonstoichiometry of high-entropy oxides [109].

An important feature of high-entropy compounds is the choice of the composition of the synthesized material. Until recently, it was believed that high-entropy compounds are only formed when cations with a close ionic radius and the same charge are used, which significantly limited the options for creating new materials. First of all, compounds with a combination of rare earth metals were used, for example, $RE_2Zr_2O_7$. However, data have been published showing that high-entropy materials can be obtained with a combination of different-valence cations [112]. The study showed that the use of oppositely charged cations satisfying the requirement of compound electroneutrality not only allows synthesizing new compounds, but also additionally stabilizes them. For example, perovskite $Ba(Zn_{0.2}Yb_{0.2}Y_{0.2}W_{0.2}Mo_{0.2})O_3$ was synthesized, i.e., Zn^{2+}, Yb^{3+}, Y^{3+}, W^{6+}, Mo^{6+} were used, which made it possible to obtain a compound with an average charge in the B-sublattice M^{4+}. This finding greatly expands the options for obtaining new high-entropy compounds.

4.3 High-entropy oxides

The bulk of the HECs considered in this section were synthesized by the standard solid-phase method. Namely, weighed portions of the initial oxides, taken in a stoichiometric ratio, are mixed in a planetary mill, and the resulting mechanical mixture is formed and sintered [119–121]. Since the porosity of the samples significantly affects their thermal and mechanical properties, spark plasma sintering can be used instead of conventional sintering to obtain ceramic samples with a density close to the theoretical one [122–124]. Less common are studies where high-entropy oxides were obtained by wet chemistry methods, such as co-precipitation [125] or combustion reactions (solution combustion synthesis: SCS) [126].

4.3.1 Pyrochlores. High-entropy pyrochlores, described by the chemical formula $A_2B_2O_7$, feature low thermal conductivity down to 0.76–0.9 W m^{-1} K^{-1} and moderate TEC up to 10.2×10^{-6} K^{-1} and Vickers hardness of $\sim$ 12.42 GPa, which significantly exceeds the values for single-component zirconates (Fig. 12) [4, 109, 127, 128]. Crack resistance of the sintered material with the $5RE_2Zr_2O_7$ composition is $\sim$ 2.24 MPa m$^{1/2}$, which is twice as high as that of $Sm_2Zr_2O_7$ and 60% higher than single-component zirco-

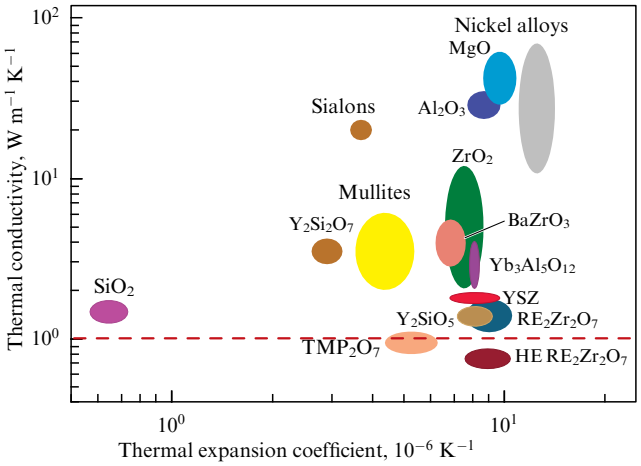

Figure 12. Comparison of high-entropy zirconates with most common materials used for TBC.

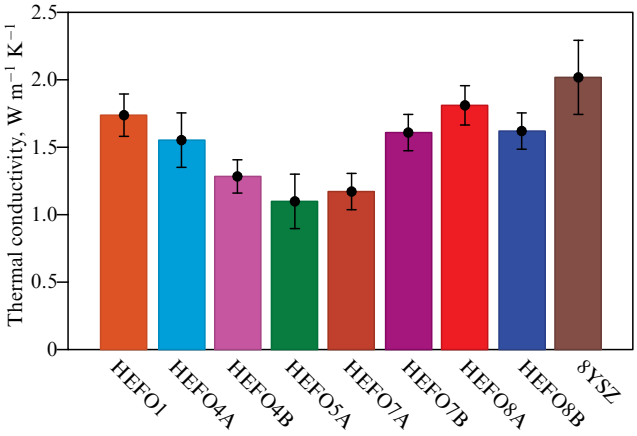

Figure 13. Comparison of thermal conductivity of high-entropy fluorites [117].

nates. This pattern may be the result of mass differences, lattice distortions, and chemical bond inhomogeneities. $5RE_2Zr_2O_7$ has the lowest thermal conductivity (0.86 W m^{-1} K^{-1}) at 1000 °C [109].

$(La_{0.2}Ce_{0.2}Nd_{0.2}Sm_{0.2}Eu_{0.2})_2Zr_2O_7$ has a thermal conductivity below 1.0 W m^{-1} K^{-1} up to 900 °C (less than half the thermal conductivity of yttria-stabilized zirconia) and a coefficient of thermal expansion close to that of nickel-based alloys [129]. The promising pyrochlore $Dy_2(Ti_{0.2}Zr_{0.2}Hf_{0.2}Ge_{0.2}Sn_{0.2})_2O_7$ [130] exhibits an estimated amorphous thermal conductivity of 1.4 W m^{-1} K^{-1} over the temperature range from room temperature to 900 °C and a coefficient of thermal expansion similar to that of nickel-based superalloys, due to which it is a promising candidate for thermal barrier coatings, for example, with possible applications in turbines. $Dy_2(Ti_{0.2}Zr_{0.2}Hf_{0.2}Ge_{0.2}Sn_{0.2})_2O_7$ is a dielectric with a resistivity of 8.10×10^{10} Ω m and a permittivity of 78 at room temperature, which is potentially interesting for use as a ceramic capacitor [130].

Important data on the effect of the deviation in the A-cation size on the formation of single-phase samples of high-entropy ceramics with the pyrochlore structure $RE_2Zr_2O_7$ are presented in [131]. It was found that, at a standard deviation of cation sizes greater than 5.2%, two-phase compounds are formed, implying that there is a maximum permissible limit in the difference between the cations used. Since high-entropy ceramics are solid solutions, a maximum difference in sizes, or deviation, by analogy with pyrochlores, should exist for all compounds of this class.

4.3.2 Fluorites. The class of high-entropy oxides that is closest to currently used YSZ, due to their identical crystal structure, are fluorites. In [117], eight single-phase fluorites of the composition $A_{0.75}B_{0.25}O_{2-d}$ were synthesized, where A = Ce^{4+}, Zr^{4+}, Hf^{4+} and B = Y^{3+}, Yb^{3+}, La^{3+}, Gd^{3+}, Ca^{2+}, Mg^{2+}, Ti^{4+} taken in different ratios. The thermal conductivity of dense ceramics of high-entropy fluorites obtained by spark plasma sintering ranged from 1.1 to 1.75 W m^{-1} K^{-1}, compared to that of YSZ obtained by the same method and equal to 2.02 W m^{-1} K^{-1} (Fig. 13). The synthesized compositions have hardness values comparable to YSZ (12.3–3.6 GPa and 13.2 GPa, respectively), despite the high content of cations that do not form hard ceramics, such as CeO_2, Y_2O_3, or Yb_2O_3. In addition, HECs with a fluorite structure feature a lower electrical conductivity than YSZ, due to which lower oxygen transport through the TBC during its operation can be expected.

In study [132], high-entropy hafnates of the composition $(Y_{0.2}Gd_{0.2}Dy_{0.2}Er_{0.2}Yb_{0.2})Hf_2O_7$ with a fluorite structure are also characterized by low thermal conductivity (0.73–0.93 W m^{-1} K^{-1}), but also low TEC (10.68×10^{-6} K^{-1}) at 1100 °C. Such low thermal conductivity is explained by the presence of a large number of vacancies, which begins to have an adverse effect at temperatures above 1000 °C and leads to an increase in thermal conductivity. The data obtained confirm the inhibitory effect of high-entropy ceramics on grain growth during sintering.

Actively studied [133–136] are $RE_2Ce_2O_7$ cerates with a fluorite structure, in which, with an increase in the cerium content Ce_{2+x}, where $x = 0.1-0.3$, thermal conductivity decreases from 2.0 to 1.6 W m^{-1} K^{-1} at 1000 °C and TEC increases from 13.49 to 13.94×10^{-6} K^{-1} [133]. The obtained Vickers hardness is 8.32–8.67 GPa [134], which exceeds the hardness for simple cerates of 3.5–5 GPa [10, 137].

The high-entropy oxide with a fluorite structure and a combination of metals in the B-sublattice $La_2(Zr_{0.2}Ce_{0.2}Hf_{0.2}Sn_{0.2}Ti_{0.2})_2O_7$ [138], despite its low thermal conductivity of 1.1 W m^{-1} K^{-1} at 800 °C, is inferior to pyrochlores and fluorites with high entropy in the A-sublattice due to a low TEC of 8.63×10^{-6} K^{-1} at 1000 °C and a growth of thermal conductivity with increasing temperature. However, due to the greater variability in doping the B-sublattice, this approach or its combination with doping of the A-sublattice appears to be the most promising one.

High-entropy oxides such as $Zr_{1-4x}Y_xTb_xTa_xNb_xO_2$ [139], $(Hf_{0.25}Zr_{0.25}Ce_{0.25}Y_{0.125}Si_{0.125})O_2$ [140], and $(Zr_{0.2}Hf_{0.2}Pr_{0.2}Y_{0.2}La_{0.2})O_2$ [141] are of particular interest because they exhibit sufficient phase stability (no changes are observed after 200-hour annealing at 1600 °C), lower thermal conductivity compared to the original YSZ (1.0–2.0 W m^{-1} K^{-1}), and at the same time a low TEC value $(8.5-11.5) \times 10^{-6}$ K^{-1} [139]. One of the disadvantages of the presented HECs is a decrease in mechanical properties (hardness and elastic modulus) compared to the original YSZ [140], which is probably due to the introduction of metals with weak metal-oxygen bonds, such as cerium.

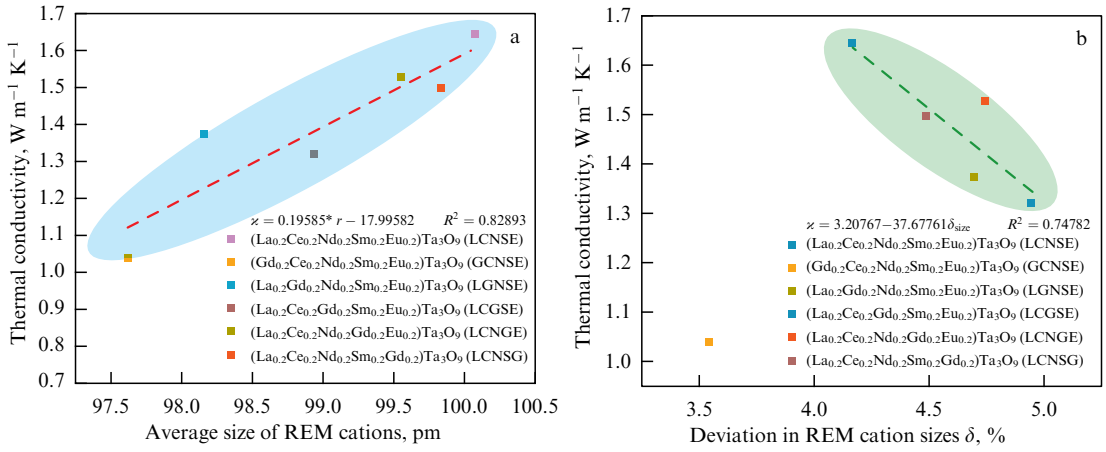

Figure 14. Dependence of thermal conductivity of high-entropy tantalates on (a) average radius and (b) size difference of rare earth cations [143].

4.3.3 Tantalates and niobates. Some high-entropy tantalates $RETa_3O_9$ and complex oxides based on them, described by the formula RE_3MO_7, where $RE = Yb_{1/3}Y_{1/3}Er_{1/3}$, M = Nb, Ta, Mo, were synthesized in studies [142, 143]. This class of compounds has a low thermal conductivity of 0.91–2.0 W m^{-1} K^{-1}, sufficient hardness of 6.9–7.93 GPa, and a TEC value significantly varying from 5.6–7.8 for pure tantalates to $(11.1-11.5) \times 10^{-6}$ K^{-1} at 800 – 1000 °C for tantalate–niobites. The observed dependence is similar to that previously found for pyrochlores: an increase in the average deviation in A-cation sizes leads to a decrease in thermal conductivity. If the entropy of materials is increased by introducing several elements into the B-sublattice, the obtained TEC decreases and the thermal conductivity of the composition increases, which is probably due to a more rigid crystal lattice (Fig. 14) [143]. The nature of the change in thermal conductivity (its increase) for all the compounds under consideration with increasing temperature shows a significant contribution of the electron component to the thermal conductivity. This implies that these compounds feature increased oxygen permeability, which will lead to active oxidation of the TBC sublayer.

4.3.4 Perovskites. High-entropy oxides with a perovskite structure were first presented in 2018 [144]. Attention was focused on obtaining compounds using elements with the same oxidation state and close atomic radii (Sn^{4+}, Zr^{4+}, Ce^{4+}, Ti^{4+}, Hf^{4+}, Mn^{4+}, Ge^{4+}, Fe^{4+}) or creating entropy in the A-sublattice. The number of possible combinations of compounds from such a small list is relatively limited, which necessitated the study of the introduction of some elements that differ in charge, such as Y^{3+} and Nb^{5+}. Using the example of titanates $ATiO_3$, medium- and high-entropy perovskites were considered in [110, 145, 146] as promising thermoelectric materials. The thermal conductivity of titanates is about 2.5 W m^{-1} K^{-1} at 1000 °C due to the significant contribution of the electronic part (specific conductivity is 10–12 kS m^{-1}). The introduction of several cations into the B-sublattice makes it possible to obtain a combination of thermophysical properties for $Sr_{0.9}La_{0.1}(Zr_{0.25}Sn_{0.25}Ti_{0.25}Hf_{0.25})O_3$ [147], which is more interesting but is still insufficient for considering such materials to be thermal barrier coatings. Thermal conductivity drops to 1.7–1.8 W m^{-1} K^{-1} at 300 °C, and then begins to increase due to the increase in the number of charge carriers (Fig. 15). Similar results were also obtained for $Sr(Zr_{0.2}Hf_{0.2}Ce_{0.2}Yb_{0.2}Y_{0.2})O_3$ [148]: initially, a high concentration of defects was created, which contributed to a sharp increase in electrical conductivity and oxygen transport in the compound. Thus, perovskite-like oxides were considered more promising materials for thermoelectrics [108, 110, 147, 149].

However, the ultra-low thermal conductivities (0.54–0.58 W m^{-1} K^{-1} [150]) obtained for dense single-crystal films of perovskite-like oxide $Ba(Zr_{0.2}Sn_{0.2}Hf_{0.2}Ti_{0.2}Nb_{0.2})O_3$ and the publication in 2021 of results showing that high-entropy oxides with a perovskite-like structure can be obtained using a combination of elements with different valences [151] made it possible to once again regard high-entropy perovskites as promising materials for TBC.

The main condition for applying the valence combination method to create new high-entropy perovskites is maintaining the electric neutrality of such compounds, which implies that the average charge of cations in the B-sublattice should be 4+ or 3+ for A^{2+} and A^{3+}, respectively. This method has significantly extended the number of existing high-entropy perovskites. However, currently, the properties and trends of their change depending on the combination of cations with different charges are hardly examined.

The data obtained on the feasibility of creating high-entropy compounds by combining cation valences can be extrapolated to other compounds (pyrochlores, fluorites, etc.), which significantly expands the options for researchers to influence the properties of the resulting compounds and the variability of the choice of composition.

5. Conclusions

The creation of new highly efficient gas turbine engines is a major technical challenge, which is primarily associated with the design of new, more advanced combustion chambers and the selection of materials for thermal barrier coatings that operate at extremely high temperatures. This task is complex, ranging from improving zirconium oxide used in industry (YSZ) and searching for more efficient alternative materials to developing new coating application methods. Moreover, the materials science task is closely related to the technological one, since the requirements for the roughness and microstructure of the sprayed coatings largely determine the requirements for the materials used and the methods of their

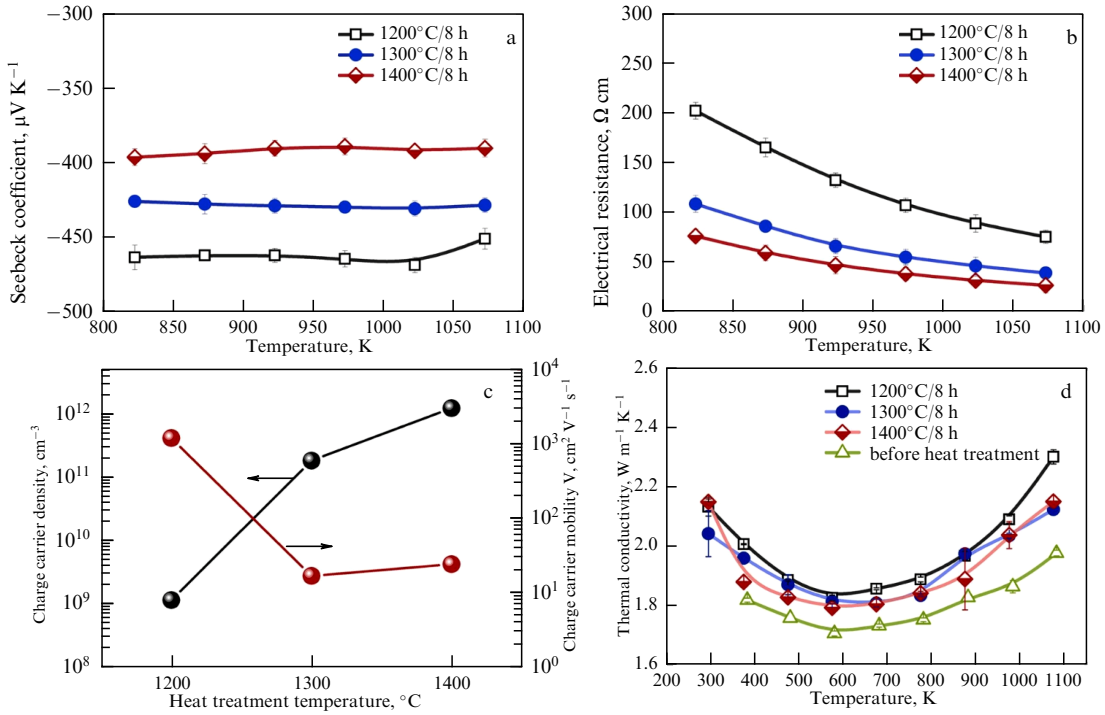

Figure 15. Temperature dependence of (a) Seebeck coefficient, (b) electrical resistance, (c) concentration and mobility of charge carriers, and (d) thermal conductivity of high-entropy titanate [147].

synthesis. As a result, a large number of research groups worldwide are actively developing new thermal barrier materials and methods to spray them.

This review presented a trend from searching for individual compounds as new thermal barrier materials to significantly complicating the chemical composition of the compounds used to obtain entropy-stabilized oxides. It should be noted that, in recent years, various high-entropy compounds have been actively studied, which yielded interesting results (for the topic under consideration): low thermal conductivity, high hardness, and phase stability. Reviewing the main areas of studies in high-entropy oxides shows promising results for a number of the compounds obtained, including pyrochlores, fluorites, and perovskites. It can be assumed that obtaining high-entropy complex oxides may be the most promising approach for further development of the technology. This choice is due to the possibility of significant improvement, first and foremost, in mechanical and thermal properties. The data presented show that it is HECs that feature lower thermal conductivity values and, usually, high hardness values compared to the simple oxides included in its composition. Due to the limited choice of refractory oxides, it seems unlikely that simple M_xO_y type oxides will be obtained, where M is an equiatomic mixture of five or more metals, since complex systems are usually more energetically advantageous. An immense impetus to further search for new highly effective materials for TBC was given by the realization of the possibility of combining cations with different valences in one sublattice. It should be noted here that it is necessary to search for the maximum permissible difference in the sizes of the cations used in the formation of complex high-entropy oxides, since, as was shown earlier, it is these compositions that exhibit the lowest thermal conductivity. Despite the variety of possible combinations, the search should be limited to metals that form refractory oxides ($T_{pl} \sim 2000\,°C$), such as Al^{3+}, Ca^{2+}, Ce^{4+}, Cr^{3+}, Hf^{4+}, Mg^{2+}, Nb^{5+}, Sc^{3+}, Sr^{2+}, Th^{4+}, U^{4+}, Zr^{4+}, Y^{3+}, REE^{3+}, which can be divided into 2 groups: cations with a large radius, which can be present in the A and B sublattices, such as Ca, Ce, Sr, Th, U, Y, REE, and other cations with a small radius. Orthorhombic perovskite-like oxides with large cations in the B-sublattice are known, such as $SrCeO_3$ and $SrPrO_3$, which have low thermal conductivity; it is possible that a combination of large cations in both sublattices will allow achieving better results. It is also worth considering the use of thorium (IV) and depleted uranium (IV), the oxides of which have high melting points and are not widely used in production industries. However, it should be taken into account that this class of compounds still has a long way to go, in terms of a thorough assessment of the operational properties and bench and industrial tests before the first real implementations.

When considering coating application methods, of particular interest, as noted earlier, are approaches using suspensions, primarily atmospheric plasma spraying. SPS makes it possible to alleviate the requirements for the source materials and to obtain alternating layers of ceramic insulating coating, which may increase the service life of gas turbine engines before major repairs. Similarly, in the case of HECs, this area of research has a long way to go in finding optimal process conditions and the most durable microstructure of sprayed coatings.

Abbreviations

- HECs — high-entropy ceramics;
- TEC — thermal expansion coefficient;
- TBCs — thermal barrier coatings;
- EB-PVD — electron beam spraying;
- HVOF — high-velocity oxygen-fuel spraying;
- S-HVOF — high-velocity oxygen-fuel spraying of suspensions;
- APS — atmospheric plasma spraying;

- SPS — atmospheric plasma spraying of suspensions;
- SPPS — atmospheric plasma spraying of precursor suspensions;
- YSH — yttria-stabilized hafnium oxide;
- YSZ — yttria-stabilized zirconium oxide.

Acknowledgments. The study was carried out as part of state assignment no. 124020600004-7.

References

1. Aleksashina A A, Podgornyi A V *Naukosfera* (5(2)) 32 (2022)
2. Cherezov A V, Grabchak E P *Nadezhnost' Bezopasnost' Energetiki* **10** 92 (2017)
3. GOST 5632-2014. Mezhgosudarstvennyi standart. Nerzhaveyushchie stali i splavy korrozionno-stoikie, zharostoikie i zharoprochnye. Marki. Izmenennaya redaktsiya. Izmenenie No. 1, s Pravkoi (GOST 5632-2014. Interstate standard. Stainless steels and alloys corrosion-resistant, heat-resistant and heat-resistant. Brands. Amended version. Amendment No. 1, with correction), https://docs.cntd.ru/document/1200113778?ysclid=lpqklnlo9p576066714, accessed December 4, 2023
4. Xiang H et al. *J. Adv. Ceram.* **10** 385 (2021)
5. Liu B et al. *J. Mater. Sci. Technol.* **35** 833 (2019)
6. Padture N P, Gell M, Jordan E H *Science* **296** 280 (2002)
7. Guy O et al. "Rapid Nanomechanical Property Mapping of Thermal Barrier Coatings" (2022), https://www.azonano.com/article.aspx?ArticleID=6229, accessed December 26, 2023
8. Vaßen R et al. *Surf. Coat. Technol.* **205** 938 (2010)
9. Bun'kova O I, Bogatova T F "Vliyanie vpryska para v gazovuyu turbinu na effektivnost' tsikla" ("The effect of steam injection into a gas turbine on cycle efficiency"), in *Energo- i Resursosberezhenie. Energoobespechenie. Netraditsionnye i Vozobnovlyaemye Istochniki Energii. Atomnaya Energetika* (Energy and Resource Saving. Energy Supply. Alternative and Renewable Energy Sources. Nuclear Power Engineering) (Eds V Yu Baldin, G I Nikitina, I S Selezneva) (Ekaterinburg: UrFU, 2018) pp. 794–797
10. Yuan J et al. *J. Alloys Compd.* **740** 519 (2018)
11. Zhang J et al. *Surf. Coat. Technol.* **323** 18 (2017)
12. Ozgurluk Y et al. *Surf. Coat. Technol.* **411** 126969 (2021)
13. Yang P et al. *Ceram. Int.* **46** 21367 (2020)
14. Dudnik E V et al. *Powder Metallurgy Metal Ceram.* **59** 179 (2020)
15. Chen D et al. *J. Therm. Spray Technol.* **32** 1327 (2023)
16. Fan W et al. *J. Eur. Ceram. Soc.* **38** 4502 (2018)
17. Xue Z et al. *J. Mater. Res. Technol.* **26** 7237 (2023)
18. Boissonnet G et al. *Surf. Coat. Technol.* **389** 125566 (2020)
19. Keyvani A et al. *J. Asian Ceram. Soc.* **8** 336 (2020)
20. Zhao P et al. *Ceram. Int.* **49** 19402 (2023)
21. Thakare J G et al. *Met. Mater. Int.* **27** 1947 (2021)
22. Chellaganesh D, Khan M A, Jappes J T W *Mater. Today Proc.* **45** 1529 (2021)
23. Sharma P, Dwivedi V K, Kumar D, in *Advances in Fluid and Thermal Engineering. Select Proc. of FLAME 2020* (Lecture Notes in Mechanical Engineering, Eds B S Sikarwar, B Sundén, Q Wang) (Singapore: Springer, 2021) p. 77, https://doi.org/10.1007/978-981-16-0159-0_8
24. Uchida N *Int. J. Engine Res.* **23** 3 (2020) https://doi.org/10.1177/1468087420978016
25. Yuan J et al. *Ceram. Int.* **47** 14515 (2021)
26. Zhang H et al. *Ceram. Int.* **46** 18114 (2020)
27. Li F et al. *J. Adv. Ceram.* **8** 576 (2019)
28. Zhou L et al. *J. Eur. Ceram. Soc.* **40** 5731 (2020)
29. Sun M et al. *Ceram. Int.* **45** 12101 (2019)
30. Zheng Q et al. *J. Alloys Compd.* **855** 157408 (2021)
31. Che J e al. *Ceram. Int.* **47** 6996 (2021)
32. Ma W et al. *J. Alloys Compd.* **660** 85 (2016)
33. Ren K et al. *J. Eur. Ceram. Soc.* **41** 1720 (2021)
34. Parchovianská I et al. *Materials* **15** 4007 (2022)
35. Praveen K et al. *Corros. Sci.* **195** 109948 (2022)
36. Zhong X et al. *J. Mater. Sci. Technol.* **85** 141 (2021)
37. Ok K M et al. *J. Eur. Ceram. Soc.* **37** 281 (2017)
38. Dharuman N et al. *Bull. Mater. Sci.* **44** 8 (2021)
39. Liu Y et al. *Mater. Res. Lett.* **7** 145 (2019)
40. Ma W et al. *J. Therm. Spray Technol.* **17** 831 (2008)
41. Ma W et al. *J. Am. Ceram. Soc.* **91** 2630 (2008)
42. Xiaoge C et al. *Ceram. Int.* **46** 14273 (2020)
43. Liu Y et al. *J. Am. Ceram. Soc.* **101** 3527 (2018)
44. Yamanaka S et al. *J. Am. Ceram. Soc.* **88** 1496 (2005)
45. Yamanaka S et al. *J. Nucl. Mater.* **344** 61 (2005)
46. Liu Y et al. *Ceram. Int.* **44** 16475 (2018)
47. Carlsson L *Acta Cryst.* **23** 901 (1967)
48. Ahtee M, Glazer A M, Hewat A W *Acta Cryst. B* **34** 752 (1978)
49. Yamanaka S et al. *J. Alloys Compd.* **352** 52 (2003)
50. Shishkin R A et al. *Ceram. Int.* **48** 27003 (2022)
51. Li C et al. *Ceram. Int.* **44** 18213 (2018)
52. Li C et al. *Ceram. Int.* **45** 21467 (2019)
53. Yu Y et al. *Ceram. Int.* **49** 25875 (2023)
54. Ren K et al. *Scr. Mater.* **178** 382 (2020)
55. Liu D et al. *J. Adv. Ceram.* **11** 961 (2022)
56. Zhu S et al. *J. Am. Ceram. Soc.* **106** 6279 (2023)
57. Guo Y et al. *J. Eur. Ceram. Soc.* **42** 6614 (2022)
58. Zhang Z et al. *J. Mater. Res. Technol.* **26** 4179 (2023)
59. Matovic B et al. *Ceram. Int.* **44** 16972 (2018)
60. Yang P et al. *Ceram. Int.* **46** 21367 (2020)
61. Vassen R et al. *J. Am. Ceram. Soc.* **83** 2023 (2000)
62. Shishkin R A *Ceram. Int.* **49** 31539 (2023)
63. Marrero-López D et al. *J. Alloys Compd.* **422** 249 (2006)
64. Sun Z et al. *J. Eur. Ceram. Soc.* **28** 2895 (2008)
65. Sun Z, Li M, Zhou Y *J. Eur. Ceram. Soc.* **29** 551 (2009)
66. Sun Z et al. *J. Am. Ceram. Soc.* **90** 2535 (2007)
67. Sun Z et al. *J. Am. Ceram. Soc.* **91** 2623 (2008)
68. Jiang B et al. *Mater. Res. Bull.* **45** 1506 (2010)
69. Xu Q-L et al. *Surf. Coat. Technol.* **398** 126093 (2020)
70. Jadhav M et al *J. Alloys Compd.* **783** 662 (2019)
71. Shahbazi H et al. *J. Therm. Spray Technol.* **33** 430 (2024)
72. Wellman R G, Deakin M J, Nicholls J R *Wear* **258** 349 (2005)
73. Dong H et al. *Surf. Coat. Technol.* **467** 129694 (2023)
74. Raza A et al. *Materials* **15** 6329 (2022)
75. Chen D *J. Therm. Spray Technol.* **31** 429 (2022)
76. Chevallier J et al. *Emergent Mater.* **4** 1499 (2021)
77. Pakseresht A H et al. *Mater. Chem. Phys.* **173** 395 (2016)
78. Shi J et al. *Chem. Eng. J.* **412** 128613 (2021)
79. Getto E et al. *Heliyon* **9** e16583 (2023) https://doi.org/10.1016/j.heliyon.2023.e16583
80. Sehhat M H, Chandler J, Yates Z *Int. J. Refract. Metals Hard Mater.* **103** 105764 (2022)
81. Lashmi P G et al. *J. Eur. Ceram. Soc.* **40** 2731 (2020)
82. Mittal G, Paul S *J. Therm. Spray Technol.* **31** 1443 (2022)
83. Pawlowski L *Surf. Coat. Technol.* **203** 2807 (2009)
84. Ganvir A et al. *J. Eur. Ceram. Soc.* **39** 470 (2019)
85. Jordan E H et al. *J. Therm. Spray Technol.* **13** 57 (2004)
86. Ma K, Tang X, Schoenung J M *J. Wuhan Univ. Technol. Mater. Sci. Ed.* **31** 35 (2016)
87. Bons J P *J. Turbomach.* **132** 021004 (2010) https://doi.org/10.1115/1.3066315
88. Pu J "Experimental simulations of effects of surface roughness level of TBC on overall effectiveness of film cooling model" *SSRN* (2022) https://doi.org/10.2139/ssrn.4235970
89. Rajasekaran B, Mauer G, Vaßen R *J. Therm. Spray Technol.* **20** 1209 (2011)
90. Sivakumar R, Mordike B L *Surf. Eng.* **4** 127 (1988) https://doi.org/10.1179/sur.1988.4.2.127
91. Leyens C et al. *Surf. Coat. Technol.* **120–121** 68 (1999)
92. Nicholls J R et al. *Surf. Coat. Technol.* **151–152** 383 (2002)
93. Sidhu T S, Prakash S, Agrawal R D *Marine Technol. Soc. J.* **39** (2) 53 (2005)
94. Mahade S et al. *Coatings* **11** 86 (2021)
95. Liu L et al. *Phys. Procedia* **18** 206 (2011)
96. Kulkarni A et al. *Mater. Sci. Eng. A* **359** 100 (2003)
97. Luo J, Stevens R *Ceram. Int.* **25** 281 (1999)
98. Movchan B A, Lemkey F D *Surf. Coat. Technol.* **165** 90 (2003)
99. Lima R S *J. Therm. Spray Technol.* **31** 396 (2022)
100. Bernard B et al. *Surf. Coat. Technol.* **318** 122 (2017)
101. Dobbins T A, Knight R, Mayo M J *J. Therm. Spray Technol.* **12** 214 (2003)

102. Zotov N et al. *Surf. Coat. Technol.* **205** 452 (2010)
103. Rätzer-Scheibe H-J, Schulz U, Krell T *Surf. Coat. Technol.* **200** 5636 (2006)
104. Li H et al. *Surf. Coat. Technol.* **182** 227 (2004)
105. Urbina M et al. *Manufacturing Rev.* **5** 9 (2018) https://doi.org/10.1051/mfreview/2018006
106. Owoseni T A "Development of nanostructured ceramic coatings from suspension and solution precursor thermal spraying process," PhD Thesis (Nottingham: Univ. Nottingham, 2021)
107. Akrami S et al. *Mater. Sci. Eng. R* **146** 100644 (2021)
108. Banerjee R et al. *ACS Sustainable Chem. Eng.* **8** 17022 (2020)
109. Wright A J, Luo J *J. Mater. Sci.* **55** 9812 (2020)
110. Zhang P et al. *J. Alloys Compd.* **898** 162858 (2022)
111. Spiridigliozzi L et al. *Acta Mater.* **202** 181 (2021)
112. Hutterer P, Lepple M *J. Am. Ceram. Soc.* **106** 1547 (2023)
113. Yang H et al. *Ceram. Int.* **48** 6956 (2022)
114. Rost C M et al. *Nat. Commun.* **6** 8485 (2015)
115. Oses C, Toher C, Curtarolo S *Nat. Rev. Mater.* **5** 295 (2020)
116. Harrington T J et al. *Acta Mater.* **166** 271 (2019)
117. Gild J et al. *J. Eur. Ceram. Soc.* **38** 3578 (2018)
118. Zhang Y et al. *Scr. Mater.* **164** 135 (2019)
119. Zhou L et al. *J. Eur. Ceram. Soc.* **40** 5731 (2020)
120. Zhao Z et al. *J. Adv. Ceram.* **9** 303 (2020)
121. Zhang D et al. *Ceram. Int.* **50** 2490 (2024)
122. Lu Y et al. *Crystals* **13** 445 (2023)
123. Zhang S et al. *Ceram. Int.* **50** 4573 (2024)
124. Biesuz M et al. *J. Asian Ceram. Soc.* **7** 127 (2019)
125. Ren K et al. *Scr. Mater.* **178** 382 (2020)
126. Cong L et al. *J. Mater. Sci. Technol.* **101** 199 (2022)
127. Wright A J et al. *J. Eur. Ceram. Soc.* **40** 2120 (2020)
128. Deng S et al. *J. Mater. Sci. Technol.* **107** 259 (2022)
129. Zhao Z et al. *J. Mater. Sci. Technol.* **35** 2647 (2019)
130. Vayer F et al. *J. Alloys Compd.* **883** 160773 (2021)
131. Yang H et al. *Ceram. Int.* **48** 6956 (2022)
132. Cong L et al. *J. Mater. Sci. Technol.* **101** 199 (2022)
133. Lilin L et al. *Ceram. Int.* **48** 14980 (2022)
134. Tang A et al. *Ceram. Int.* **48** 5574 (2022)
135. Haoming Z et al. *Ceram. Int.* **48** 8380 (2022)
136. Zhang H et al. *Ceram. Int.* **48** 1512 (2022)
137. Liu K et al. *Mater. Sci. Eng. A* **625** 177 (2015)
138. Zhang D et al. *Ceram. Int.* **48** 1349 (2022)
139. Yao Y, Yang F, Zhao X *J. Am. Ceram. Soc.* **105** 35 (2021)
140. Liew S L et al. *J. Alloys Compd.* **904** 164097 (2022)
141. Zhang F et al. *J. Mater. Sci. Technol.* **105** 122 (2022)
142. Sun G, Wang W, Sun X *Ceram. Int.* **48** 8589 (2022)
143. Li C et al. *Ceram. Int.* **48** 11124 (2022)
144. Jiang S et al. *Scr. Mater.* **142** 116 (2018)
145. Yu P et al. *Ceram. Int.* **48** 15992 (2022)
146. Zhou S et al. *Chem. Eng. J.* **427** 131684 (2022)
147. Lou Z et al. *J. Eur. Ceram. Soc.* **42** 3480 (2022)
148. Zhan H et al. *Int. J. Appl. Ceram. Technol.* **20** 1764 (2022)
149. Zhang P et al. *J. Mater. Sci. Technol.* **97** 182 (2022)
150. Sharma Y et al. *Phys. Rev. Materials* **2** 060404 (2018)
151. Tang L et al. *J. Am. Ceram. Soc.* **104** 1953 (2021)